Composites Part B 177 (2019) 107401

Contents lists available at ScienceDirect

Composites Part B

journal homepage: www.elsevier.com/locate/compositesb

Preparation of low-κ polyimide resin with outstanding stability of dielectric properties versus temperature by adding a reactive Cardo-containing diluent

Xiuting Li, Peiyan Zhang, Jie Dong **, Feng Gan, Xin Zhao, Qinghua Zhang *

Key Laboratory of High Performance Fibers & Products, Ministry of Education, Donghua University, Shanghai, 201620, PR China

ARTICLE INFO

Keywords:
Polyimide
Cardo-containing diluent
Low dielectric constant
Dielectric stability
Cross-linking

ABSTRACT

High stability of low-κ value in a broad temperature region is a critical property for low dielectric constant polymer materials especially when they are served in some harsh conditions. However, most polymer dielectrics always exhibit a significant variation in dielectric property at around T_g or sub-T_g due to the local segment or chains motion, thus, low-κ polymer dielectrics are limited to a relatively narrow working temperature region. Herein, we described a series of novel crosslinked polyimide (PI) thermosets by blending a reactive Cardo-containing diluent into the PI oligomer, the dielectric constants of which were greatly reduced from 3.4 to 2.5 and were surprisingly stable over a temperature region of -150-250 °C. Meanwhile, the cured blended thermosets exhibited a 32–139 °C increase in T_g compared to the pristine PI. Detailed analyses have illustrated that the significantly reduced κ value, highly stable dielectric property and superior stability of these blended samples are originated from the synergistic effects of the large free-volume of Cardo-containing diluent, looser molecule packing resulted from the TR reaction and the highly crosslinked network. This desirable combination of facile processability, attractive dielectric behavior and excellent thermal stability makes them potential utilization in aerospace, microelectronic industries and other harsh environment applications.

1. Introduction

Polyimide (PI) thermosetting resins, a contender to epoxy, dicyanate ester and polybenzoxazine used as the matrix in continuous fiber reinforced polymer composites (CFRP) [1] or as the substrate materials for producing ultralarge scale integration (ULSI) circuits [2,3], gained much interest due to their excellent thermal stability, good mechanical properties, superior radiation resistance, nonflammability, good chemical resistance and so on. Another dazzling characteristic of polyimide thermosets is their rich molecular design flexibility and easily functionalized allowing for designing various structures to meet the application requirements [4–6]. For example, with continuing miniaturization in the dimensions of electronic devices utilized in ULSI circuits, high-performance polyimide substrates with a low dielectric constant (κ) and good thermal stability are now urgently required, which play a dominant role in reducing the resistance-capacitance delay, crosstalk noise and power dissipation of electronic devices. In addition, such low dielectric PI resins also have an important application in broadband radar-wave-transparent composites to minimize the loss of interfere electromagnetic wave transmission [7].

Decreasing the dipole strength or the number of dipoles (increasing the free volume) or a combination of both has been proved as the main approaches to scale down the dielectric constant of polymers [8]. For instance, incorporation of some less polarizable units, including C–Si, C–F and Si–Si bonds into the polymer backbone is meaningful for reducing the polarizability of molecules, in which the most common way is fluorination of materials. For example, Fang et al. [9] reported a new structural fluoropolymer PFN containing a perfluorocyclobutane group, which exhibited a dielectric constant of 2.33 with a dielectric loss less than 1.2×10^{-3} at a high frequency of 30 MHz due to the abundant less polar C–F group and loose molecular stacking. Huang et al. [10] prepared a novel polyimide with the κ value below 2.5 by introducing the perfluorocyclobuty (PFCB) unit into the polyimide backbone, which simultaneously endowed the PI with some of the lowest water uptake of 0.065%. Generally, the incorporation of fluorine substituents into a polyimide can decrease its dielectric constant of 2.5–3.0, and an

* Corresponding author.
** Corresponding author.
E-mail addresses: dj01@dhu.edu.cn (J. Dong), qhzhang@dhu.edu.cn (Q. Zhang).

https://doi.org/10.1016/j.compositesb.2019.107401
Received 9 July 2019; Received in revised form 29 August 2019; Accepted 29 August 2019
Available online 3 September 2019

ancillary benefit to fluorination in polyimides seems to be the decreased water absorption, which endows polyimides an excellent durability of low-κ value even in a moisture circumstance for a prolonged period of time [11]. However, some major issues with the fluorinated polyimides can not be ignored including the high cost of the fluorine monomers and the fact that adhesion of polyimides is always compromised relative to unfluorinated materials, which dramatically limit this technique for a practical use.

As an alternative method, introduction of controlled porosity in materials also has been widely applied for developing ultra-low dielectric materials. Meador et al. [12] prepared a series of highly porous polyimide aerogels by the supercritical CO_2 drying process and the dielectric constant was decreased to as low as 1.16, which was successfully utilized as the substrate to fabricate patch antennas with a broad bandwidth and higher gain than the commercial substrates. In addition, incorporating nanoporous polyhedral oligomeric silsesquioxanes (POSS) [13] and phosphotungstic acid (PWA) [14] also has been illustrated as a workable way to prepare low dielectric polymer materials. In general, the κ value of porous materials can be less than 2.0, however, the precise controlling sizes and distribution of pores remains a challenging work. Another drawback of this method is that the high content of pores easily results in a dramatically deterioration of mechanical properties and significant water uptake. Therefore, the development of non-porous polyimide materials by adopting some less-polar and hydrophobic monomers with a large free volume instead of the introduction of pores seems to be a more effective method.

For most low-κ polyimide materials, another easily neglected drawback is their unsatisfied constancy of dielectric property in a broad temperature region. For example, Khazaka et al. [15] reported that the dielectric constant of polyimide derived from the BPDA and ODA was featured as a double-peak characteristic at a relatively low frequency in the heating process from −150 °C to 370 °C. Similar result also has been found on the commercial Matrimid® polyimide [16]. Electric devices containing ULSI circuits or radars equipped with the wave-transparent composites will definitely experience high/low temperatures or be applied under different frequencies, the poor stability of dielectric behavior will be troublesome for the low-κ polyimides. Numerous studies [17,18] have revealed that glass or sub-glass relaxation processes, β and γ relaxations, were the origins of dielectric constant fluctuation below the T_g. For the γ transition (usually located at < -50 °C), the residual water in the polymers appears to play an important role, and a direct correlation between water content and the intensity of the relaxation has been demonstrated. In the case of β relaxation of polyimides (in the temperature region of 50–200 °C), different mechanisms have been proposed involving the local motions of polymer chains, encompass larger portions of the repeat unit that respond in a correlated manner. In light of the above mentioned analysis, it seems that reducing the water absorption of polyimides and restricting the local repeat segment motion of polymer chains will make a significance on limiting theγand β relaxations and be meaningful for improving the dielectric stability of polymeric materials. In fact, as an example, Sun et al. [19] successfully synthesized a fluorinated and cross-linked polyhedral oligomeric silsesquioxane (POSS). This hybrid polymer exhibited a stable and low dielectric constant (<2.56) and low dissipation factor ($<3.1 \times 10^{-3}$) in a wide range of frequencies from 40 Hz to 30 MHz and even at a high frequency of 5 GHz attributed to the fluorination and cross-linking of molecular design strategies. However, as far as we know, full dense polyimide materials with a stable ε-value below 3.0 in the high frequency and temperature region have rarely been reported.

In this work, we reported a facile method by blending a reactive and thermally-rearranged able (TR) Cardo-containing diluent (Cardo-HPI) into a polyimide oligomer to address the issues of simultaneously scaling down the dielectric constant and improving the dielectric stability and thermal resistance of polyimide materials. Primarily, with the simple addition of Cardo-HPI, an obvious decrease in the dielectric constant is observed and is hypothesized to arise from both the increased free volume and reduced polymer chains polarity. Moreover, the homogeneous materials exhibit an excellent dielectric stability in a broad frequency and temperature region ($f = 100$ MHz to 1 GHz, $T = -150$-250 °C) compared to the pristine PI oligomer. The detailed synthetic strategy, the microstructures and properties of the resultant materials are discussed in detail.

2. Experimental section

2.1. Materials

9,9-bis(4-hydroxylphenyl)fluorene (BisHPF) was purchased from Adamas Reagent Co., Ltd. 4,4′-Bis(3-aminophenoxy) benzophenone (BABP), 2,3,3′,4′-biphenyltetracarboxylic dianhydride (α-BPDA) and 4-Phenylethynylphthalic anhydride (PEPA) were all supplied by Changzhou Sunlight Pharmaceutical Co., Ltd (Changzhou, China). N-methyl-2-pyrrolidone (NMP) was purchesed from Ling Feng Chemicals Co., Ltd. (Shanghai, China). Other chemicals such as Pd/C (10% Pd), hydrazine hydrate, acetone, concentrated nitric acid and ethanol are all reagent grade and obtained from Sinopharm Chemical Reagent Co. Ltd.

2.2. Synthesis of 9,9-bis(3-amino-4-hydroxyphenyl) fluorene diamines (BisAHPF) and the 9,9-bis(3-(3-phenylethynyl) phthalimide-4-hydroxyphenyl) fluorene (Cardo-HPI)

The synthesis and structures of BisAHPF and Cardo-HPI are shown in Scheme 1(A). Herein, the intermediate component BisAHPF was prepared according to Lu's previous work [20] *via* a two-step synthetic route including the nitration and reduction reactions using the 9,9-bis (4-hydroxylphenyl)fluorene as the starting material. Firstly, 6.00 g BisHPF was dissolved in 30 mL acetone in a 250 mL flask equipped with a stirrer. 6.00 g concentrated nitric acid was added into the flask slowly by a constant pressure funnel. The reaction solution was cooled to 4 °C and kept for 12 h. Then, some yellow powder was precipitated as adding 30 mL cooled water into the solution. The solid powder was washed several times by ethanol and dried under vacuum. Finally, about 4.50 g solid powder was obtained. About 4.5 g 9,9-bis(3-nitro-4-hydroxyphenyl)fluorene intermediate was dissolved in 30 mL ethanol. Then, 0.5 g Pd/C (10 wt%) and 30 mL hydrazine hydratewas added into the solution under a constant pressure. The solution was stirred at 60 °C for 12 h. After that the Pd/C was removed by filtration and deionized water was added into the solution, and about 3.6 g BisAHPF powder could be obtained after washing and drying. The diluent Cardo-HPI was derived from the BisAHPF and PEPA. As an example, in a 100 mL three-necked flask equipped with a mechanical stirrer, a thermometer, and a dean stark trap were added BisAHPF (6.69 g, 0.018 mol) and PEPA (8.73 g, 0.036 mol) in N-methly-2-pyrrolidone (NMP, 60 ml). The mixture was stirred for 5 h at room temperature under nitrogen. Then, toluene (5 mL) was added, and the mixture was heated to 185 °C for 6 h, in which the byproduct water evolved in the thermal imidization was simultaneously removed from the reaction system by azeotropic distillation. The resultant mixture was poured into an excess of deionized water to yield precipitate. The solid was collected by filtration, washed by ethanol twice and dried in a vacuum oven at 80 °C for 6 h to give a white powder. Yield: 13.2 g (85.5%). FTIR (KBr, cm^{-1}): 3304 (-OH), 2212 (C≡C), 1779 and 1718 (C═O), 1376 and 748 (C–N). ^{1}H NMR (DMSO-d_6, 400 MHz): δ = 9.89 (s, 2H), 8.02–8.00 (m, 4H), 7.93–7.91 (m, 4H), 7.65 (m, 4H), 7.50–7.48 (m, 8H), 7.40 (t, 2H, J = 9.6), 7.34 (m, 2H, J = 9.6), 7.09–7.06 (m, 4H), 6.91 (d, 2H, J = 5.6 Hz). Anal. Calcd for $C_{57}H_{32}N_2O_6$: C, 81.42%; H, 3.84%; N, 3.33%. Found: C, 80.90%; H, 3.87%; N, 3.22%.

2.3. Synthesis of polyimide oligomer (PI oligomer)

The phenylethynyl-terminated PI oligomer with the calculated polymerization degree of $n = 4$ was synthesized by BABP, α-BPDA and PEPA in NMP according to a typical synthesis route as shown in Scheme

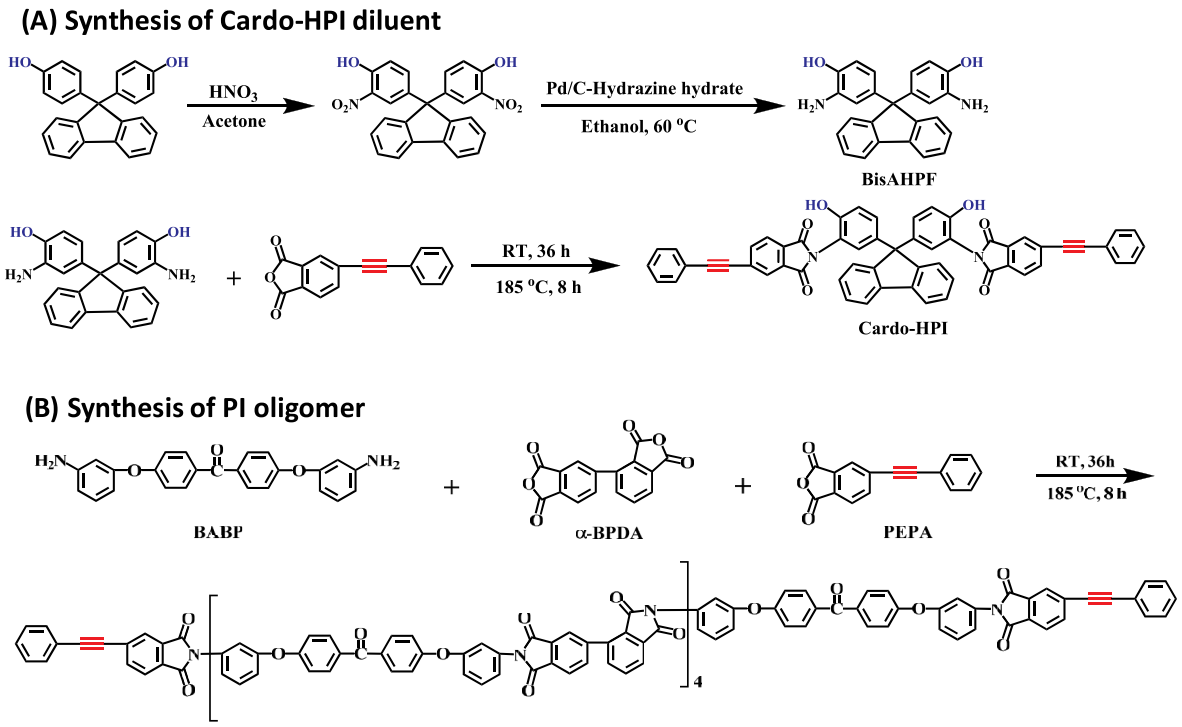

Scheme 1. (A) Synthesis route of Cardo-HPI diluent and (B) PI oligomer with the repeat unit $n = 4$.

1(B). BABP (21.24 g, 0.054 mol) and α-BPDA (13.51 g, 0.046 mol) dispersed in NMP (130 ml) were added in a dried 250 ml three necked round-bottom flask and stirred at 60 °C for 12 h to yield a viscous poly (amic acid) solution. Subsequently, PEPA (3.80 g, 0.015 mol) with some extra NMP (20 ml) was added and the mixture was heated and refluxed at 185 °C for 8 h, in which the precursor poly(amic acid) was transformed to polyimide. After cooling down, the resulting solution was poured into the deionized water and yellow powder was obtained by filtration and drying procedures under vacuum with the yield of 91.2%. FTIR (KBr, cm^{-1}): 2212 (C≡C), 1772 and 1715 (C═O), 1371 and 743 (C–N), 1240 (-O-). Anal. Calcd. for $C_{221}H_{120}N_{10}O_{35}$: C, 76.38%; H, 3.45%; N, 4.03%. Found: C, 80.90%; H, 3.87%; N, 3.22%. Molecular weight: $M_n = 4473\ g\ mol^{-1}$, $M_w = 7380\ g\ mol^{-1}$, polydispersity index (PDI) = 1.65.

2.4. Preparation of PI oligomer/Cardo-HPI blends and the cured resins

PI/Cardo-HPI blends with various Cardo-HPI concentrations were prepared by a simple physical solution mixing. A certain amount of PI oligomer/Cardo-HPI blends were dissolved in NMP with a solid content of 15 wt% and stirred for 6 h at room temperature, and then a homogenous solution containing PI oligomer and Cardo-HPI was obtained. The corresponding films were prepared by casting the solution on a glass plate and dried in a vacuum oven at 100 °C for 12 h. In the curing process, the solid films were slowly heated up to 120, 150, 250 and 350 °C for each 1 h, respectively, and finally at 370 °C for 1.0 h under a pressure of 2 MPa. In a similar way, PI/Cardo-HPI mixtures containing 5, 10, 20, 30 and 40 wt% of Cardo-HPI were obtained and abbreviated as PI/Cardo-X (X represented the content of Cardo-HPI).

2.5. Characterization

The ^1H NMR and ^{13}C NMR of the Cardo-HPI diluent were recorded on a Bruker Avance 400. Meanwhile, for the thermally rearranged Cardo-HPI, the solid state CP-MAS (cross-polarisation/magic angle spinning) ^{13}C NMR spectra were recorded at a frequency of 600 Hz. Chemical shifts were calculated relative to TMS. The spectra were acquired with 5 s recycle delays, and the number of transients was 3000. Molecular weights were measured by gel permeation chromatography (PL-GPC 50) with polystyrene as an external standard and dimethylacetamide (DMAc) as the eluent. Fracture morphologies of the PI/Cardo-HPI mixture films were characterized by a FESEM (HITACHI S-4800). FTIR spectra were obtained on a Nicolet 8700 spectrometer in the range of 4000–500 cm^{-1}. Differential scanning calorimetry (DSC) was tested on a TA DSC Q20 at a scan rate of 10 °C/min in flowing nitrogen. Rheological measurements were performed on a HAAKE MARS III Rotational Rheometer with a fixed strain of 5% and angular frequency of 10 rad/s. Specimen discs with the diameter and thickness of 20 mm and 2.0 mm, respectively, were prepared by press-molding (2 MPa) the oligomer powders at the room temperature. Complex viscosity (η^*) was measured from 100 to 400 °C at a heating rate of 4 °C/min under a continuous nitrogen flow. Dynamic mechanical properties and the dimensional stabilities of cured mixture films were characterized by the DMA Q800 (TA Instruments). Wide-angle X-ray diffractometry (WAXD) spectra were conducted in the reflection mode at room temperature by using a Rigaku Dmax-2550 diffractometer with Cu Kα radiation (λ = 1.54 Å). Thermal gravity analysis (TGA) was performed on a Netzsch TG 209 F3 thermal analysis system in N_2 with a heating rate of 10 °C/min. Positron annihilation lifetime spectroscopy (PALS) was utilized to characterize the free volume cavity size and distribution of the resultant resins. Dielectric properties were tested by Agilent E4991A impedance analyzer at various frequencies. Dielectric behaviors of samples in the heating or cooling process were measured by a Novocontrol Concept 40 high-resolution alpha dielectric analyzer.

3. Results and discussion

3.1. Synthesis of Cardo-HPI

In this study, a novel reactive diluent Cardo-HPI containing Cardo, *ortho*-hydroxy imide and phenylethynyl moieties was designed and synthesized according to Scheme 1(A). Series of polymers containing bis

(phenyl)fluorene as the Cardo moieties have been intensively reported [21,22], and these polymers intended to exhibit good thermal stabilities, excellent solubilities and transparency as well as low dielectric constants due to the rigid chemical structure with a relatively high free volume of Cardo. For the *ortho*-hydroxy imide unit, which has a nucleophilic functional hydroxyl group in the *ortho* position of the imide ring, can be thermally rearranged (TR) into a heteroaromatic benzoxazole group. During the structural rearrangement of materials in the solid state, the distortion of the imide moiety into a rigid-rod heterocyclic benzoxazole ring always leads to the formation of microcavity with diameters ranging from 3 Å to 9 Å and an obvious increased molecular free volume, which is advantageous from the low-dielectric point of view [23]. Moreover, aromatic polymers containing benzoxazole rings always have excellent thermal stabilities and are less prone to water absorption than the polyimides. Besides, the thermally initiated phenylethynyl group in Cardo-HPI is expected to form chemical links with the phenylacetylene-terminated polyimide matrix and modify the cross-linking networks in the system so as to improve the dielectric stability of cured resins.

The chemical structure of Cardo-HPI was confirmed by ^{1}H NMR and ^{13}C NMR analyses. As shown in Fig. 1(A), the characteristic proton resonance attributed to the hydroxy is observed at 9.9 ppm. Additionally, the ^{1}H NMR spectra conforms the presence of phthalimide unit as observed by the presence of the proton resonance at 7.93 and 8.01 ppm, respectively. Also, the appearance of peak signals of H_a, H_b and H_c indicates the incorporation of phenylethynyl moiety into the Cardo-HPI. In Fig. 1(B), the characteristic resonances at 166.6 (C_3), 153.3 (C_2), 93.9 (C_5), 88.6 (C_4) and 63.5 (C_1) ppm for carbon atoms of phthalimide, hydroxyl-linked phenyl, phenylethynyl and Cardo groups, further illustrate the successful synthesis of the target Cardo-HPI compound.

3.2. Morphological analysis and the hydrogen-bonding interaction of PI/Cardo-HPI blends

The miscibility of PI/Cardo-HPI blends with different Cardo-HPI concentrations can be visualized by direct morphological analysis. Fig. 2 shows the SEM images of fractured morphologies of blends with the indicated Cardo-HPI loading. Clearly, all samples show similar fracture surfaces to the neat PI oligomer, and no obvious phase separation was observed, suggesting the formation of homogeneous blends. Therefore, it is speculated that there must be some special interactions or linkages that randomly linking the PI oligomer matrix and the Cardo-HPI.

In view of the chemical structures of PI oligomer and Cardo-HPI, abundant C═O bond of imide rings in PI oligomer and free phenolic OH groups in Cardo structure offer a favorable condition for hydrogen-bonding interaction. The ATR-FTIR was utilized to investigate the intrinsic interaction between the PI oligomer and Cardo-HPI. Fig. 3(A) displays the FTIR spectra (4000-650 cm^{-1} region) of the PI/Cardo-HPI blends of various weight ratios. All samples are featured absorption bands at around 1720 and 1381 cm^{-1} representing the imide C═O symmetric stretching and imide C–N stretching indicating the successful formation of imide moieties. The obvious characteristic absorption band at 2212 cm^{-1} conforms the presence of phenylethynyl group, whose intensity increases with the amount of Cardo-HPI. Additionally, a broad band around 3400 cm^{-1} representing the O–H characteristic peak in all blends and Cardo-HPI, which is always regarded as the typical signal for intermolecular hydrogen bonding interaction [24], gradually increases upon increasing the Cardo-HPI concentration. An investigation of the reason for miscibility was conducted in perspective of the hydrogen-bonding interaction by characterizing the bands shifts of the O–H (*ca.* 3400 cm^{-1}) and C═O (*ca.* 1720 cm^{-1}). Representative O–H stretching spectra is shown in Fig. 3(B) in the region of 3700–3000 cm^{-1}. The hydroxy band is observed at 3445 cm^{-1} in PI/Cardo-5 and linearly shifts to 3425 cm^{-1} at 30 wt% Cardo-HPI in the blend, and meanwhile, the characteristic band becomes stronger and broader with the increased Cardo-HPI concentration. In addition, as shown in Fig. 3(C), the carbonyl stretching near 1720 cm^{-1} is also lowered about 5 cm^{-1}. Previous studies by Lu et al. [25] have illustrated that a significant shift of C═O and X–H (X = C, N, O and S) would occur upon the formation of hydrogen-bonding interaction. Actually, hydrogen-bonding interaction has been illustrated as the crucial physical factor that directly determining the miscibility of two totally different polymers such as the polybenzimidazole (PBI)/PIs [26], poly(L-lactide)/poly(4-vinylphenol) (PLLA/PVPh) [27], poly(benzoxazine imide)/PVPh [28] and so on. Thus, the FTIR results conform that the hydrogen bonding (C═O···H–O) has formed and been enhanced after blending the Cardo-HPI in PI oligomer, which makes a great contribution to the miscibility of the blends.

3.3. Thermal properties and rheological behavior of the uncured PI/Cardo-HPI blends

Fig. 4 exhibits the DSC thermograms of the uncured PI oligomer/Cardo-HPI blends containing different concentrations of Cardo-HPI. The DSC profile of the neat PI oligomer features a T_g at around 193 °C and an exothermic peak having a maximum temperature of 414 °C representing the cross-linking reaction of phenylethynyl groups. For all blends, the single T_g further illustrates that the Cardo-HPI is dispersed uniformly in the PI matrix and stabilized through the C═O···H–O hydrogen-bonding interaction. Obviously, the T_g values of the PI/Cardo-HPI blends decreases from 184 °C to 162 °C upon increasing the content of Cardo-HPI from 5 to 40 wt%, indicating that the Cardo-HPI acts as a low molecular plasticizer presented in the system. The addition of linear, tribranched or hyperbranched plasticizer into polymers to reduce their T_gs has been frequently observed in many miscible blends, such as PLA/

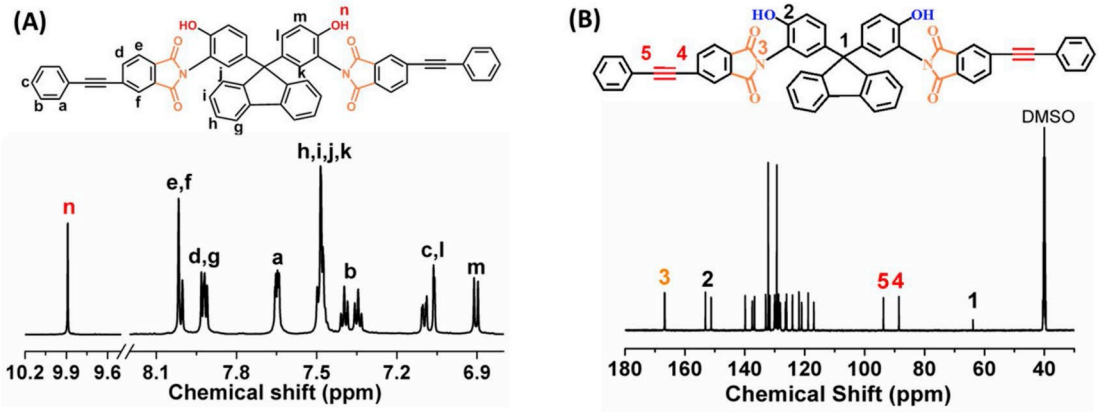

Fig. 1. (a) ^{1}H NMR and (B) ^{13}C NMR spectra of Cardo-HPI.

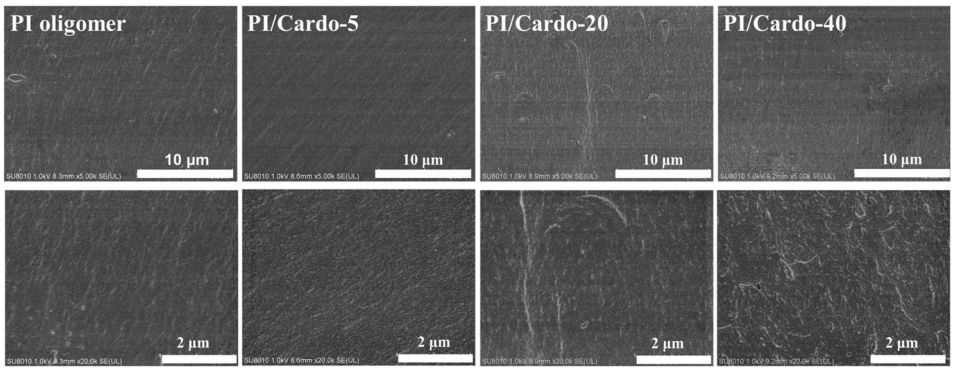

Fig. 2. SEM images of cross-section of uncured PI oligomer precursors with different Cardo-HPI contents.

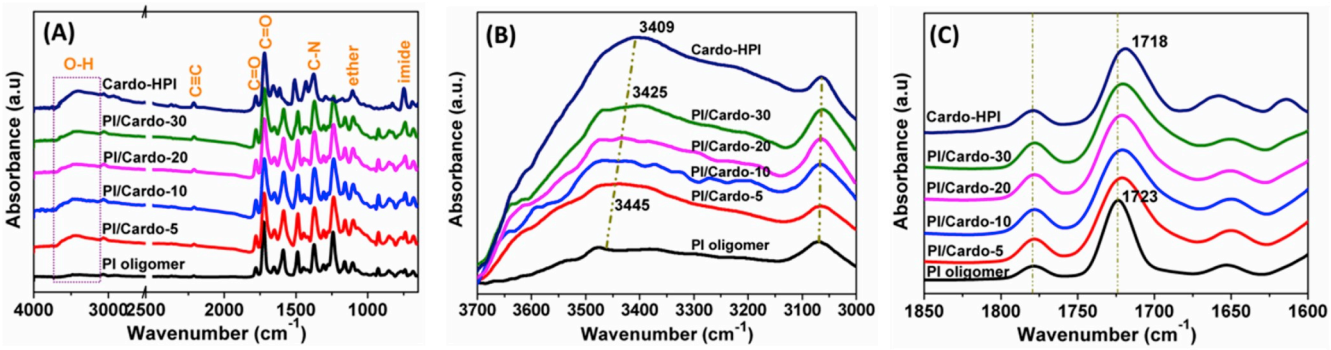

Fig. 3. (A) ATR-FTIR spectra of uncured PI oligomer precursors containing different content of Cardo-HPI diluent; (B) and (C) magnified ATR-FTIR spectra in the range of 3700–3000 cm^{-1} and 1850-1600 cm^{-1}, respectively.

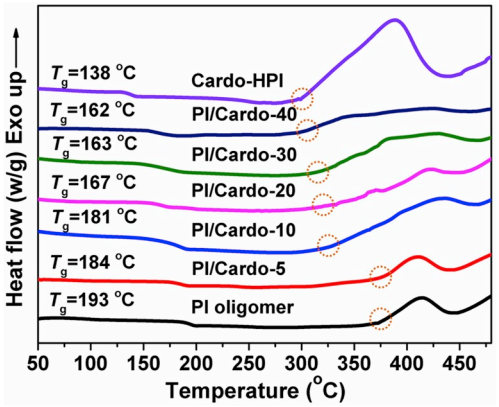

Fig. 4. DSC thermograms of the uncured PI oligomer/Cardo-HPI blends of various weight ratios.

PEG [29], epoxy-phenolic/HBPSi [30] and so on, and has been recognized as an important approach to optimizing the processing property of many plastics or polymer resins in the industrial application. In this contribution, the reduction of 10–30 °C in the T_g of blends is expected to bring some advantageous for the processing performance of PI resins. Another interesting phenomenon in the DSC curves is that the cross-linking reaction tends to start in a lower temperature and completes in a wider temperature region as evidenced by a broader exothermic peak for the blends with respective to the pristine PI, which is mainly attributed to that the addition of Cardo-HPI increases the concentration of phenylacetylene per unit mass of blends.

The rheological behaviors of the uncured Cardo-HPI-containing oligomers and the pristine PI oligomer were investigated. As revealed in Fig. 5(A), the minimum melt viscosity of Cardo-HPI was only 1.65 Pa s at 268 °C, which is much lower than that of the pristine PI (3.8 Pa s at 306 °C) attributed to its relatively low molecule weight and the lateral fluorene group with a large free volume. The complex viscosity $|\eta^*|$ of the PI/Cardo-HPI blends *versus* temperature is shown Fig. 5(B). Clearly, the blends exhibit a similar rheological behavior as the Cardo-HPI concentration is lower than 10 wt%. While, continuously increasing the Cardo-HPI content, the blends exhibit higher viscosities than that of the pristine PI before the oligomer reaching the minimum viscosity, which is mainly attributed to the strengthened hydrogen-bonding interaction between the Cardo-HPI and PI oligomer that severely limiting the mobility of polymer chains. As increasing temperature, the $|\eta^*|$ drops faster and the samples containing 20, 30 and 40 wt% of Cardo-HPI exhibit the minimum viscosities of 3.6 Pa s at 303 °C, 2.9 Pa s at 300 °C and 2.7 Pa s at 294 °C, respectively, which are lower than the minimum viscosity of the pristine PI oligomer. It has been illustrated that the hydrogen-bonding interaction is sensitive to the temperature, and this physical interaction can be destroyed under a high temperature condition [31]. Thus, we can reasonably assign the quickly decreased viscosities of PI/Cardo-HPI blends to the dissociation of the intermolecular hydrogen bonds. It is noted that the incorporation of Cardo-HPI resulting in the lower minimum melt viscosity of these oligomers makes a great significant for their melt processability. In addition, as shown in Fig. 5(B), all blends show high viscosities than the pristine PI in the high temperature region, which are mainly attributed to the followed cross-linking reaction of phenylethynyl group and thermally-rearrangement of *ortho*-hydroxy imide unit to the rigid benzoxazole group. Detailed analysis is discussed in the following.

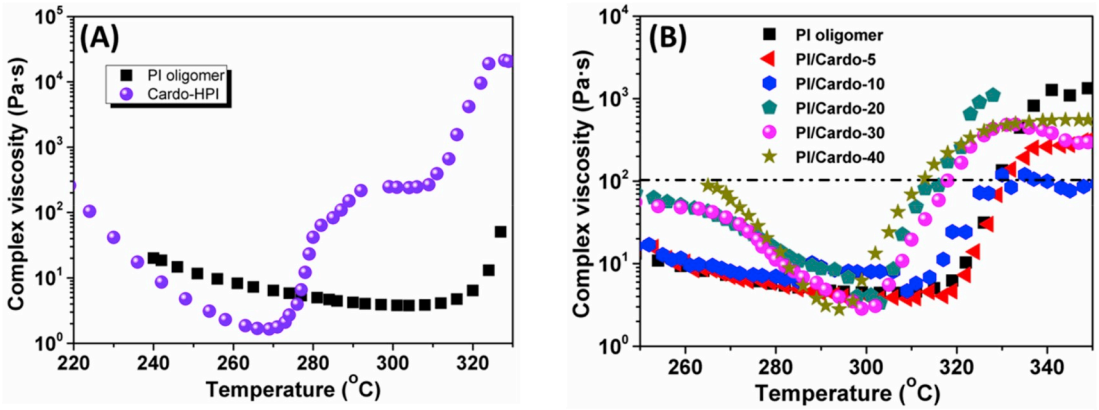

Fig. 5. (A) Complex melt viscosity of the uncured PI oligomer and Cardo-HPI; (B) complex melt viscosity of uncured PI oligomer/Cardo-HPI blends of various weight ratios.

3.4. Thermally-rearrangement of Cardo-HPI and the PI/Cardo-HPI blends

As mentioned above, aromatic polyimides with the *ortho*-hydroxy group can be thermally rearranged (TR) to heteroaromatic polybenzoxazoles (PBOs), which is significant for improving the thermal stability and adhesion to metal surface of TR polymers. Moreover, the dielectric constants of PBOs fall in the range of 2.6–3.0 due to the intrinsic less polarizable benzoxazole groups, which make them attractive for many applications. Herein, the *ortho*-positioned hydroxy group on the imide rings of Cardo-HPI is fully qualified for the thermal rearrangement reaction. As shown in Fig. 6(A), a two-step weight loss in TGA can be distinguished for the Cardo-HPI: an initial mass loss occurring at 300–400 °C and a second weight loss ranging from 400 to 650 °C. In fact, the cross-linking reaction of phenylethynyl group in Cardo-HPI also takes place in the temperature region of 300–400 °C [32], however, the crosslinking of phenylethynyl groups belongs to a typical thermo-additional polymerization and no obvious change in weight loss can be detected. Using the TGA-FTIR, it can be illustrated that only CO_2 leaves during the first weight loss step (Supplementary Fig. S1). Thus, the first mass loss is associated with the thermal rearrangement of Cardo-HPI. In order to qualitatively study the structural evolution of Cardo-HPI during heating, FTIR analyses were carried out. As shown in Fig. 6(B), clearly, the hydroxy-containing imide structure and the phenylethynyl unit remain stable to 200 °C as seen by the appearance of characteristic imide carbonyl at 1773 and 1727 cm^{-1} and the C≡C group at around 2201 cm^{-1}, respectively. However, when rising the temperature to 370 °C, almost complete cross-linking reaction

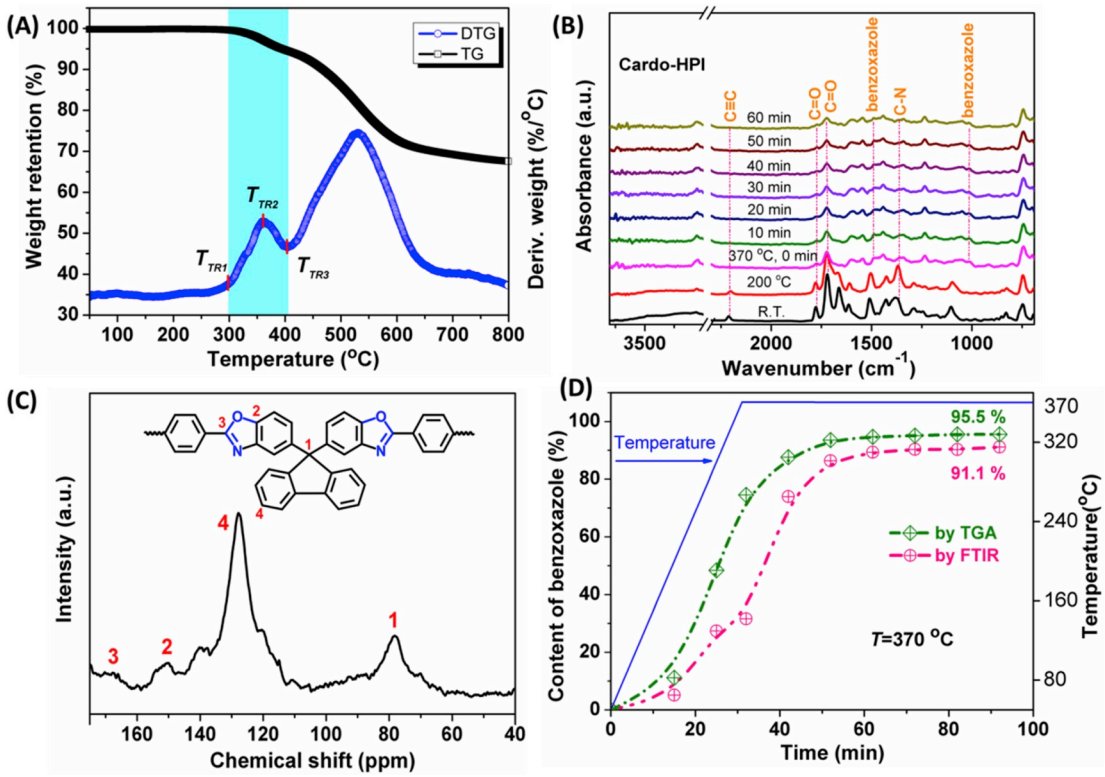

Fig. 6. (A) Thermal rearrangement analysis by TGA for the Cardo-HPI in the temperature range of 50–800 °C, (B) FTIR spectra of Cardo-HPI thermally treated from room temperature to 370 °C and kept for various time, (C) solid-state ^{13}C NMR of thermally rearranged Cardo-HPI and (D) content of benzoxazole unit formed in the TR reaction of Cardo-HPI determined by TGA and FTIR.

is observed as evidenced by the disappearance of C≡C, and meanwhile, conversion of the hydroxy-containing imide to aromatic benzoxazole occurs due to the decreased intensity of imide carbonyl at 1773 cm^{-1} and the appearance of benzoxazole ring stretching at 1012 cm^{-1}. For obtaining more detailed information about the thermally treated Cardo-HPI, as reported in some previous works [33–35], CP-MAS ^{13}C NMR spectra was recorded for the sample treated at 370 °C for 1.0 h. As shown in Fig. 6(C), a peak for benzoxazole at 167 ppm (C_3) and Cardo unit at 78 ppm (C_1) are present in the spectra further conforming the formation of benzoxazole moiety. Based on the above analyses, detailed degrees of conversion under 370 °C for different times can be obtained by measuring the actual weight loss in TGA or the increased intensity in FTIR spectra. As shown in Fig. 6(D), the TR reaction is characterized by a initial rapid stage and a slow one in the late stage, and the Cardo-HPI reaches 95.5% and 91.1% conversion at 370 °C for 1.0 h measured by TGA and FTIR, respectively. Jo et al. [36] have reported that there was a strong relationship between the chain rigidity and thermal conversion behavior. Thus, in this work, the gradually increased molecule rigidity of Cardo-HPI leads to the slow and incomplete conversion.

The TGA and DTG curves of PI/Cardo-HPI blends with different Cardo-HPI concentrations are shown in Fig. S2. All thermograms present a distinct weight loss in the range of 275–400 °C, and the weight loss corresponding to this process differs for different compositions and increases as the mass fraction of Cardo-HPI. Meanwhile, as shown in Fig. S2(B), diverse Cardo-HPI contents did not show important differences in the temperature region of thermal rearrangement for all blends, which indicates that the Cardo-HPI in different blends has a similar conversion behavior.

3.5. Structures and properties of the cured PI/Cardo-HPI thermosets

When treated at 370 °C for 1.0 h, PI/Cardo-HPI oligomers were transformed to cured thermosets because of the thermal cross-linking of phenylethynyl groups, and over 90% hydroxy-containing imide units were thermally rearranged to aromatic benzoxazole moieties. The X-ray diffraction profiles of the cured thermosets are shown in Fig. 7. All samples show a broad amorphous halo, indicating a typical amorphous nature of all these polymers. Moreover, the content of Cardo-HPI in samples clearly changes the position of the amorphous halo maximum. In detail, the maximum peak of cured pristine PI is located at 21°, meaning a average intersegmental distance of around 0.40 nm. It can be easily appreciated that the average interchain distances for all blends have notably increased with the concentration of Cardo-HPI. For instance, the maximum peak for the PI/Cardo-HPI-40 shifts to $2\theta = 18°$ with the corresponding *d*-spacing value of 0.47 nm, indicating a lower chain packing-density for these cured thermosets. On one hand, the nonplanar lateral fluorene group in Cardo-HPI may lead to a structural disorder and contribute to the increased intermolecular distance. On the other hand, as reported before for TR polymers [37], thermal rearrangement of hydroxy-containing imide or amide to benzoxazole group always resulted in the increased *d*-spacing values and free volumes. Herein, as illustrated in Fig. 7(B), an amorphous halo maximum at $2\theta = 19.1°$ for the Cardo-HPI, corresponding to a *d*-spacing value of 0.46 nm, gradually shifts to $2\theta = 17.5°$ for the TR-Cardo-HPI with the *d*-spacing value of 0.51 nm, further illustrating a looser molecule packing structure for the TR polymer. Furthermore, PALS was carried out to quantitatively analyze the effect of incorporated Cardo-HPI on the average free volume of these thermosets. As shown in Fig. S3, the orthopositronium (*o*-Ps) has a longer lifetime (τ_3) and higher intensity (I_3) in PI/Cardo-20 than the cured pristine PI resin before its annihilation. As we know, the lifetime and intensity of the annihilation are indicative of the size and concentration of the cavity in the materials. Thus, based on the Eqs. S(1) and S(2), the fraction of free volume of 0.45% and 0.62% can be calculated for the cured pristine PI and PI/Cardo-20 thermosets, respectively. Therefore, the incorporation of Cardo-HPI into the PI oligomer contributes to a less packed and more disordered structure for this set of rigid-rod polymer thermosets, favorable in reducing their dielectric constant and dielectric loss.

Thermal dynamic mechanical properties of the resultant thermosets are shown in Fig. 8 and Table 1. As shown in Fig. 8(A), incorporating the Cardo-HPI into the PI oligomer has dramatically improved the storage modulus (E') and the rapid attenuation of the E' shifts to a higher temperature region (from 240 °C for the pristine PI to 275 °C for the PI/Cardo-30), indicating their increased dynamical mechanical properties. In Fig. 8(B), T_g taken from the peak temperature of Tan δ curves ranges from 271 to 402 °C and increases with the content of Cardo-HPI. For example, the PI/Cardo-30 exhibits 108 °C higher in T_g than that of the pristine PI. Typically, aromatic polymers, such as polyimide (PI), polybenzoxazole (PBO), polybenzimidazole (PBI), *etc*, are difficult to be processed, while, the exceptionally easy processability of the current PI/Cardo-HPI blends with excellent thermal stabilities makes them a great potential for various applications in some harsh conditions, such as in aerospace, automobile and microelectric industries and many other fields.

As for the PI/Cardo-HPI system, its curing mechanism contains the triple bond addition of phenylethynyl groups in PI oligomer and Cardo-HPI, and it is reasonably speculated that this addition reaction may occur between PI and Cardo-HPI and result in chemical linkages, providing a guarantee for outstanding thermal stability, dimensional stability and mechanical properties. The values of cross-linking density V_e for the cured PI/Cardo-HPI were estimated by the classical equation based on the statistical theory as shown in following [38,39]:

$$V_e = E'/6RT \quad (1)$$

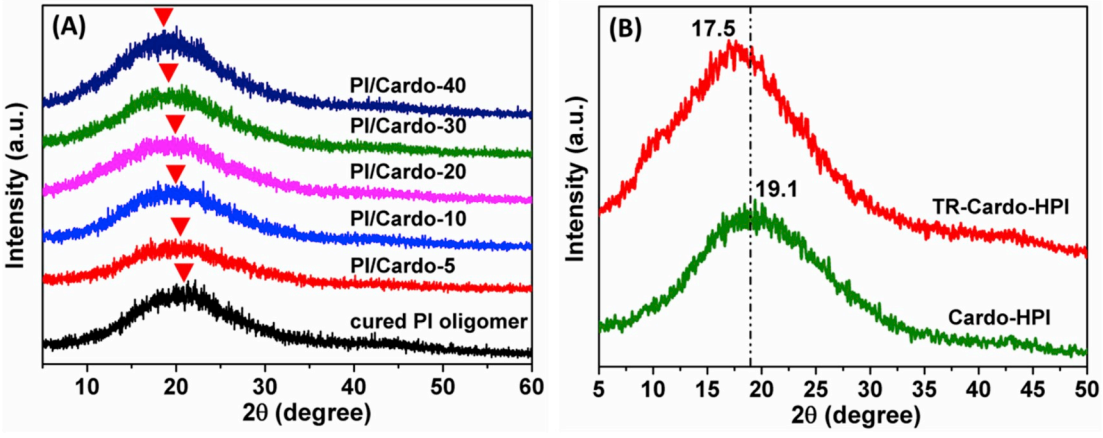

Fig. 7. (A) WAXD curves of cured PI/Cardo-HPI thermosets of various Cardo-HPI contents and (B) WAXD patters of cured pristine PI and TR-Cardo-HPI.

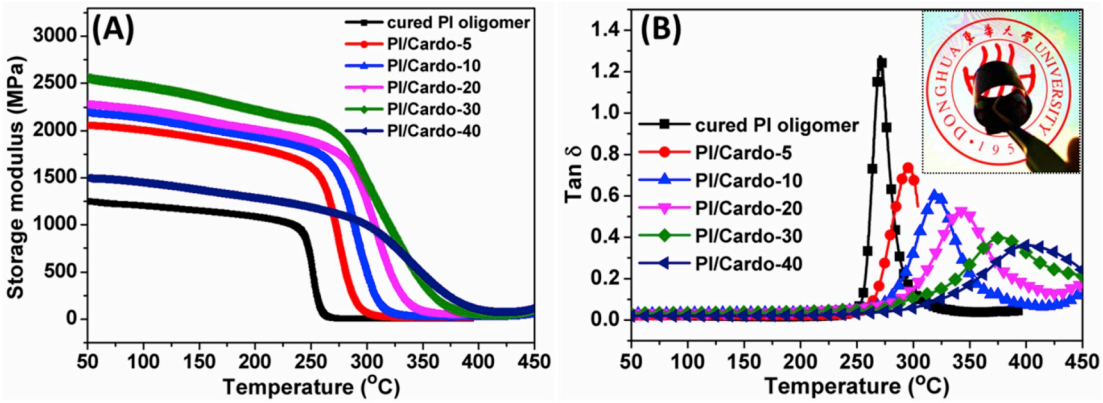

Fig. 8. Storage modulus (A) and Tan δ curves (B) of cured PI/Cardo-HPI thermosets with different Cardo-HPI contents.

Table 1
Thermal dynamic mechanical properties of cured PI/Cardo-HPI thermosets.

Samples	T_g[a] (°C)	E'[b] (MPa)	V_e[c] (10^3 mol/cm^3)	CTE[d] (ppm/°C)
PI oligomer	264	4.5	1.6	37.3
PI/Cardo-5	296	17.3	5.7	36.8
PI/Cardo-10	323	18.7	5.9	33.2
PI/Cardo-20	343	22.2	6.8	31.4
PI/Cardo-30	378	47.7	13.8	29.2
PI/Cardo-40	403	96.7	27.1	28.1

[a] Measured by DMA at a heating rate of 5 °C/min; the peak temperature of the tan δ curve.
[b] E' refers to the storage modulus determined at $T = T_g + 40$ K.
[c] V_e refers to the cross-linking density.
[d] CTE values were measured by DMA under the DMA controlled force model.

where E' represents the storage modulus of the cured resin in the rubbery plateau region, which is always chosen as the modulus at $T = T_g + 40$ K. R is the gas constant. The detailed values of cross-linking density for cured PI/Cardo-HPI thermosets are listed in Table 1. Obviously, the V_e increases linearly with the content of Cardo-HPI. For PI/Cardo-30, the V_e reaches around 6.8×10^3 mol/cm^3, which is nearly 4.3 times of that of the cured pristine PI. The inserted picture in Fig. 8(B) shows a rolled sample of PI/Cardo-20 demonstrating its flexibility even though the high cross-linking density. While, continually increasing the Cardo-HPI content to 40 wt% in the blends, the V_e is up to 27.1×10^3 mol/cm^3, which results in a serious brittleness to the sample and severely limits its applications.

Thermal dimensional stability is an important issue for polymer resins because they are always laminated with other metals or ceramic substrates for the thermal processing. Given the cross-linking network structure in the blends, it can be expected the thermal dimensional stability of the thermosets would get a high reinforcement by the homogeneous dispersion of Cardo-HPI. As illustrated in Table 1, the CTE decreases with the increasing Cardo-HPI content, and the CTE lower than 30 ppm/K is obtained from the cured thermosets containing more than 30 wt% Cardo-HPI. The dramatically increased cross-linking density predominantly reduces the chains mobility of PI and thus suppresses the thermal expansion of the materials.

Fig. 9 reveals the thermal stabilities of the thermosets containing different contents of Cardo-HPI. The initial thermal decomposition temperature (T_i) and the 5 wt% weight loss decomposition temperature (T_{d5}) range from 440 to 452 °C and 459–470 °C, respectively, in a nitrogen atmosphere, and samples with a higher content of Cardo-HPI seem to be more thermally stable. Gu et al. [40–42] reported the "heat-resistance index" (T_{HRI}) was another parameter that could reflect and reveal the "thermal stability" of polymers or polymer composites. Based on their previous studies, T_{HRI} values of the thermosets in this work were also calculated and results were listed in the inserted table, which

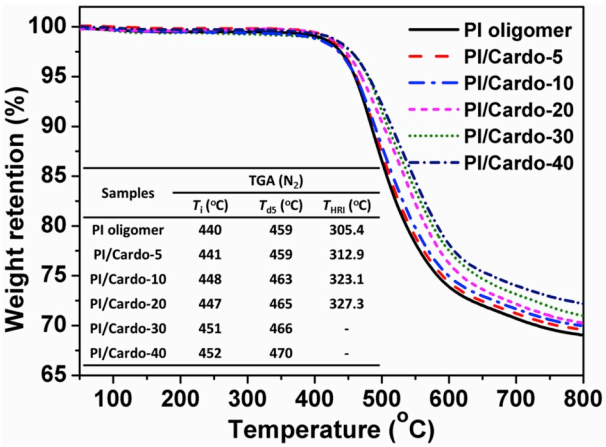

Fig. 9. TGA curves of cured PI/Cardo-HPI thermosets in nitrogen.

increased from 305.4 °C for the pristine PI to 327.3 °C for the PI/Cardo-20 thermoset. It indicated that the thermal stability of the blended thermosets was obviously enhanced. Two factors are responsible for these results. Firstly, the incorporation of Cardo-containing diluent with a rigid chemical structure may account for the enhanced thermal stability of the blends. The second one is the increased cross-linking density.

Mechanical properties of the thermally treated PI/Cardo films were measured and the results were shown in the Fig. S4. Obviously, in Fig. S4 (A), the resultant thermoset containing 10 wt% Cardo-HPI exhibits the highest tensile strength of 149 MPa, approximately 50% higher than that of the cross-linked PI oligomer, demonstrating that the addition of moderate concentration of Cardo-HPI is beneficial for preparing a robust PI thermoset. While, as the mass concentration of Cardo-HPI is over 10 wt%, the tensile strength and elongation at break of the thermosets decrease dramatically. Particularly, the PI/Cardo-40 has a tensile strength of only 17 MPa and an elongation at break of 1.7%, while, it still shows a rolled film as shown in the inserted picture of Fig. S4(B).

The dielectric constant and dielectric loss of cured PI/Cardo-HPI thermosets as a function of frequency and temperature are presented in Fig. 10. As shown in Fig. 10(A), the dielectric constant of the cured pristine PI is around 3.4 at 100 MHz, which is comparable to most common PI resins falling in the range from 3.0 to 3.5. As expected, the prepared thermosets display considerably lower dielectric constants depending on the content of Cardo-HPI. Upon incorporating 20 wt% of Cardo-HPI, the cured resin exhibits a κ value of 2.7 and steadily decreases to 2.5 at 100 MHz as continuously increasing the Cardo-HPI to 40 wt%, revealing that the addition of Cardo-containing diluent can substantially reduce the dielectric constant of PIs by a simple blending

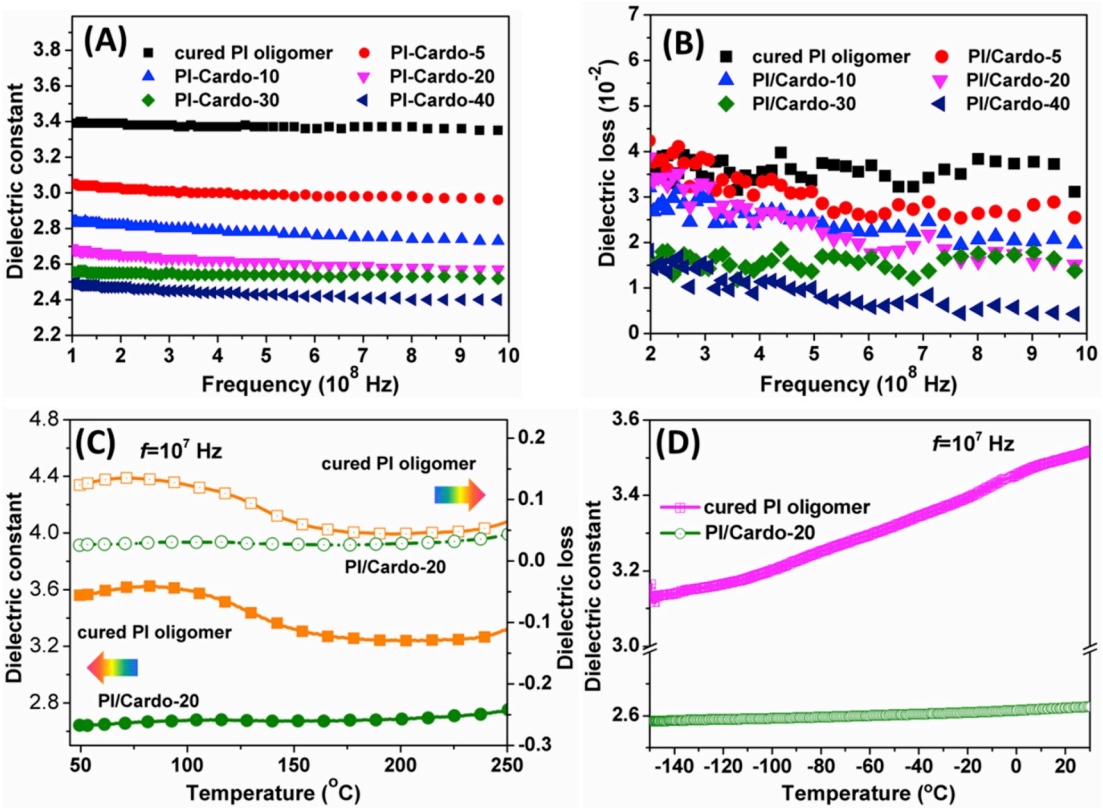

Fig. 10. (A) Dielectric constant and (B) dielectric loss versus frequency of cured PI/Cardo-HPI thermosets, (C) comparison of the dielectric constant and dielectric loss versus temperature between the cured pristine PI oligomer and the PI/Cardo-20 thermoset and (D) comparison of the cured PI and PI/Cardo-20 thermosets measured at a low-temperature region from −150 to 25 °C.

method. Besides, the dielectric constants of these cured thermosets are even lower than or comparable to those of other PI composites containing some particular nanofillers (*e.g.* graphene oxide (GO) [43], hyperbranched polysiloxane (HBPSi) [44] and so on). Meanwhile, as presented in Fig. 10(B), the dielectric loss of these blends stays at a low scale ranging from 0.01 to 0.04, and increasing the Cardo-HPI content is meaningful for reducing the dielectric factor.

As we know, dielectric materials in aerospace or in microelectronics are always required to enable the use in ultralow or high temperature applications, which makes a high requirement for the dielectric stability of these materials. However, at temperatures approaching T_g or sub-T_g, polymers easily lose their dimensional and electromechanical stability and display large variations in dielectric properties with temperatures. For instance, the biaxially oriented polypropylene (BOPP), the best commercially available polymer can operate only at temperatures below 105 °C [45]. In this work, we examine the dielectric constant and dielectric loss as a function of temperature. As shown in Fig. 10(C), at $f = 10^7$ Hz, a minor variation in κ with temperature, that is ranging from 2.65 to 2.74 within the temperature range of 45–250 °C, while the cured pristine PI, shows a κ variation from 3.6 to 3.2. Of particular interest is that the cured pristine PI exhibits a significant fluctuation in κ and in dielectric loss at 45–150 °C, which is just like a dielectric relaxation process. Comparatively, this relaxation can not be observed in the PI/Cardo-20. For gaining a deeper understanding of this result, the enlarged Tan δ curves in the dynamic mechanical measurements are provided and shown in Fig. S5. Obviously, a second relaxation peak at around 70 °C (the β relaxation) for the cured pristine PI can be observed. Therefore, the fact that the dielectric-constant-maximum peak appears at around 79 °C for the pristine PI is due to the β relaxation of PI chains. However, the blended thermosets do not exhibit this β relaxation, indicating that addition of Cardo-HPI is meaningful for suppressing the secondary relaxation of these glassy polymers. As reported in previous work [15], the β relaxation for polyimides is related to the phenyl ring, imide group and other dipolar motions, and may be influenced by the water absorption. As illustrated in Table 1, incorporating Cardo-HPI into the PI matrix can dramatically suppress the chains mobility by forming a highly cross-linked network structure, and thus, resulting in the reduction of dipole alignment motion. Actually, Wang et al. [45] previously reported a similar approach for preparing flexible dielectric materials by highly cross-linking the polymer chains with the boron nitride nanosheets, and the dielectric properties of resultant nanocomposites are extraordinarily stable even at 300 °C, further illustrating the validity of cross-linking method for improving the stability of dielectric properties. Herein, dielectric behaviors of the prepared thermosets in the low temperature region were also investigated. As shown in Fig. 10(D), the dielectric constant of the pristine PI increases from 3.1 to 3.5 as the temperature increasing from −150 to 25 °C, with a variation of 13%. While, a minor variation in κ with temperature, that is <1.6%, is seen in PI/Cardo-20, indicating that the introduction of crosslinkable Cardo-HPI also makes a great contribution to improve the dielectric stability in the low-temperature region, which makes it feasible to be used as dielectric materials in a wide range of application.

Water absorption behavior makes a great effect on the materials' dielectric properties. Generally, high water uptake of the material always leads to poor stability of dielectric property, which is particularly troublesome for low dielectric constant materials. The corresponding water absorption rates and water contact angle values of the resultant thermosets were measured and the results were shown in Fig. S6. The pristine PI exhibits a water absorption and water contact angle of 3 wt% and 76°, respectively. When incorporating Cardo-HPI into the PI oligomer, the hydrophobicity of the resultant thermosets is dramatically enhanced, e.g., the water uptake of PI/Cardo-40 decreases to only 1.1 wt %, mainly attributed to the better hydrophobicity of benzoxazole structure. The remarkable moisture resistance is a highly valuable

property for these thermosets.

4. Conclusions

A reactive Cardo-containing diluent has been successfully synthesized and was blended with the PI oligomer. Miscibility was suggested by the observation of homogeneous morphologies and single composition dependent T_gs of the blends, and the hydrogen-bonding interaction was illustrated to play a dominant role in the compatibility between the Cardo-HPI diluent and the PI oligomer matrix. A similar advantage of reducing the minimum melt viscosity of the PI oligomer by incorporating Cardo-HPI was observed as other diluents or plasticizers. Meanwhile, the Cardo-HPI was shown to simultaneously undergo a thermally rearrangement and cross-linking reaction in the thermal treatment of the blends. The formation of less polarizable benzoxazole moieties and the cross-linked networks combined with the bulky fluorene groups of Cardo-HPI endowed the resultant thermosets with some exceptional properties, such as the low dielectric constant ($\kappa = 3.4$–2.4 at 100 MHz), excellent stability of low-κ value in a broad temperature region ($T = -150$-$250\,^{\circ}C$) and excellent thermal stability ($T_g = 264$–$403\,^{\circ}C$), making them as the extremely promising raw materials for high performance thermosets.

Acknowledgements

This work was supported by the Program of Shanghai Academic Research Leader (18XD1400100), National Natural Science Foundation of China (No. 21774019), the Fundamental Research Funds for the Central Universities (2232019G-02) and the Fundamental Research Funds for the Central Universities and Graduate Student Innovation Fund of Donghua University (CUSF-DH-D-2019009).

Appendix A. Supplementary data

Supplementary data to this article can be found online at https://doi.org/10.1016/j.compositesb.2019.107401.

References

[1] Hassanzadeh-Aghdam MK, Ansari R, Darvizeh A. Micromechanical modeling of thermal expansion coefficients for unidirectional glass fiber-reinforced polyimide composites containing silica nanoparticles. Compos Part A: Appl S 2017;96:110–21.
[2] Jeon H, Yoon C, Song YG, Han J, Kwon S, Kim S, et al. Reducing the coefficient of thermal expansion of polyimide films in microelectronics processing using ZnS particles at low concentrations. ACS Appl Nano Mater 2018;1(3):1076–82.
[3] Park S, Chang HY, Rahimi S, Lee AL, Tao L, Akinwande D. Transparent nanoscale polyimide gate dielectric for highly flexible electronics. Adv Electron Mater 2018;4(2):1700043.
[4] Liaw DJ, Wang KL, Huang YC, Lee KR, Lai JY, Ha CS. Advanced polyimide materials: syntheses, physical properties and applications. Prog Polym Sci 2012;37(7):907–74.
[5] Guo Y, Yang X, Ruan K, Kong J, Dong M, Zhang J, et al. Reduced graphene oxide heterostructured silver nanoparticles significantly enhanced thermal conductivities in hot-pressed electrospun polyimide nanocomposites. ACS Appl Mater Interfaces 2019;11(28):25465–73.
[6] Guo Y, Lyu Z, Yang X, Lu Y, Ruan K, Wu Y, et al. Enhanced thermal conductivities and decreased thermal resistances of functionalized boron nitride/polyimide composites. Compos B Eng 2019;164:732–9.
[7] Gu J, Li Y, Liang C, Tang Y, Tang L, Zhang Y, et al. Synchronously improved dielectric and mechanical properties of wave-transparent laminated composites combined with outstanding thermal stability by incorporating iysozyme/POSS functionalized PBO fibers. J Mater Chem C 2018;6(28):7652–60.
[8] Zhao XY, Liu HJ. Review of polymer materials with low dielectric constant. Polym Int 2010;59(5):597–606.
[9] Yuan C, Jin K, Li K, Diao S, Tong J, Fang Q. Non-porous low-*k* dielectric films based on a new structural amorphous fluoropolymer. Adv Mater 2013;25(35):4875–8.
[10] Jia M, Li Y, He C, Huang X. Soluble perfluorocyclobutyl aryl ether-based polyimide for high-performance dielectric material. ACS Appl Mater Interfaces 2016;8(39):26352–8.
[11] Volksen W, Miller RD, Dubois G. Low dielectric constant materials. Chem Rev 2010;110(1):56–110.
[12] Meador MAB, Wright S, Sandberg A, Nguyen BN, Van Keuls FW, Mueller CH, et al. Low dielectric polyimide aerogels as substrates for lightweight patch antennas. ACS Appl Mater Interfaces 2012;4(11):6346–53.
[13] Geng Z, Huo M, Mu J, Zhang S, Lu Y, Luan J, et al. Ultra low dielectric constant soluble polyhedral oligomeric silsesquioxane (POSS)-poly(aryl ether ketone) nanocomposites with excellent thermal and mechanical properties. J Mater Chem C 2014;2(6):1094–103.
[14] Geng Z, Ba J, Zhang S, Luan J, Jiang X, Huo P, et al. Ultra low dielectric constant hybrid films via side chain grafting reaction of poly(ether ether ketone) and phosphotungstic acid. J Mater Chem 2012;22(44):23534–40.
[15] Khazaka R, Locatelli M, Diaham S, Bidan P, Dupuy L, Grosset G. Broadband dielectric spectroscopy of BPDA/ODA polyimide films. J Phys D Appl Phys 2013;46(6):065501.
[16] Comer AC, Kalika DS, Rowe BW, Freeman BD, Paul DR. Dynamic relaxation characteristics of Matrimid® polyimide. Polymer 2009;50(3):891–7.
[17] Comer AC, Ribeiro CP, Freeman BD, Kalakkunnath S, Kalika DS. Dynamic relaxation characteristics of thermally rearranged aromatic polyimides. Polymer 2013;54(2):891–900.
[18] Chisca S, Musteata VE, Sava I, Bruma M. Dielectric behavior of some aromatic polyimide films. Eur Polym J 2011;47(5):1186–97.
[19] Wang J, Sun J, Zhou J, Jin K, Fang Q. Fluorinated and thermo-cross-linked polyhedral oligomeric silsesquioxanes: new organic-inorganic hybrid materials for high-performance dielectric application. ACS Appl Mater Interfaces 2017;9(14):12782–90.
[20] Lu Y, Hao J, Li L, Song J, Xiao G, Zhao H, et al. Preparation and gas transport properties of thermally induced rigid membranes of copolyimide containing cardo moieties. React Funct Polym 2017;119:134–44.
[21] Kazama S, Teramoto T, Haraya K. Carbon dioxide and nitrogen transport properties of bis(phenyl)fluorene-based cardo polymer membranes. J Membr Sci 2002;207(1):91–104.
[22] Nakabayashi K, Imai T, Fu MC, Ando S, Higashihara T, Ueda M. Poly(phenylene thioether)s with fluorene-based Cardo structure toward high transparency, high refractive index, and low birefringence. Macromolecules 2016;49(16):5849–56.
[23] Tena A, Rangou S, Shishatskiy S, Filiz V, Abetz V. Claisen thermally rearranged (CTR) polymers. Sci Adv 2016;2(7):e1501859.
[24] Lee H, Mensire R, Cohen RE, Rubner MF. Strategies for hydrogen bonding based layer-by-layer assembly of poly(vinyl alcohol) with weak polyacids. Macromolecules 2012;45(1):347–55.
[25] Lian M, Lu X, Lu Q. Synthesis of superheat-resistant polyimides with high T_g and low coefficient of thermal expansion by introduction of strong intermolecular interaction. Macromolecules 2018;51(24):10127–35.
[26] Ahn TK, Kim M, Choe S. Hydrogen-bonding strength in the blends of polybenzimidazole with BTDA-and DSDA-based polyimides. Macromolecules 1997;30(11):3369–74.
[27] Zhang L, Goh SH, Lee SY. Miscibility and crystallization behaviour of poly(l-lactide)/poly(*p*-vinylphenol) blends. Polymer 1998;39(20):4841–7.
[28] El-Mahdy AF, Kuo SW. Direct synthesis of poly (benzoxazine imide) from an ortho-benzoxazine: its thermal conversion to highly cross-linked polybenzoxazole and blending with poly (4-vinylphenol). Polym Chem 2018;9(14):1815–26.
[29] Pillin I, Montrelay N, Grohens Y. Thermo-mechanical characterization of plasticized PLA: is the miscibility the only significant factor? Polymer 2006;47(13):4676–82.
[30] Liu H, Zhang J, Gao X, Huang G. Simultaneous reinforcement and toughness improvement of an epoxy-phenolic network with a hyperbranched polysiloxane modifier. RSC Adv 2018;8(32):17606–15.
[31] Liu T, Peng X, Chen YN, Bai QW, Shang C, Zhang L, et al. Hydrogen-bonded Polymer-small molecule complexes with yunable mechanical properties. Macromol Rapid Commun 2018;39(9):1800050.
[32] Li X, Liu T, Jiao Y, Dong J, Gan F, Zhao X, et al. Novel high-performance poly(benzoxazole-*co*-imide) resins with low dielectric constants and superior thermal stabilities derived from thermal rearrangement of ortho-hydroxy polyimide oligomers. Chem Eng J 2019;359:641–51.
[33] Meador MAB, Johnston JC, Cavano PJ. Elucidation of the cross-link structure of nadic-end-capped polyimides using NMR of 13C-labeled polymers. Macromolecules 1997;30(3):515–9.
[34] Nakamura K, Ando S, Takeichi T. Thermal analysis and solid-state ^{13}C NMR study of crosslink in polyimides containing acetylene groups in the main chain. Polymer 2001;42(9):4045–54.
[35] Roberts CC, Apple TM, Wnek GE. Curing chemistry of phenylethynyl-terminated imide oligomers: synthesis of ^{13}C-labeled oligomers and solid-state NMR studies. J Polym Sci, Polym Chem Ed 2000;38(19):3486–97.
[36] Jo HJ, Soo CY, Dong G, Do YS, Wang HH, Lee MJ, et al. Thermally rearranged poly(benzoxazole-co-imide) membranes with superior mechanical strength for gas separation obtained by tuning chain rigidity. Macromolecules 2015;48(7):2194–202.
[37] Calle M, Lee YM. Thermally Rearranged (TR) Poly(ether-benzoxazole) membranes for gas separation. Macromolecules 2011;44(5):1156–65.
[38] Kumar KS, Nair CR, Ninan K. Investigations on the cure chemistry and polymer properties of benzoxazine-cyanate ester blends. Eur Polym J 2009;45(2):494–502.
[39] Zhuo D, Gu A, Liang G, Hu Jt, Yuan L, Chen X. Flame retardancy materials based on a novel fully end-capped hyperbranched polysiloxane and bismaleimide/diallylbisphenol A resin with simultaneously improved integrated performance. J Mater Chem 2011;21(18):6584–94.
[40] Gu J, Lv Z, Wu Y, Guo Y, Tian L, Qiu H, et al. Dielectric thermally conductive boron nitride/polyimide composites with outstanding thermal stabilities via in-situ

polymerization-electrospinning-hot press method. Compos Part A: Appl S 2017;94:209–16.
[41] Yang X, Guo Y, Han Y, Li Y, Ma T, Chen M, et al. Significant improvement of thermal conductivities for BNNS/PVA composite films via electrospinning followed by hot-pressing technology. Compos B Eng 2019;175:107070.
[42] Yang X, Guo Y, Luo X, Zheng N, Ma T, Tan J, et al. Self-healing, recoverable epoxy elastomers and their composites with desirable thermal conductivities by incorporating BN fillers *via* in-situ polymerization. Compos Sci Technol 2018;164:59–64.
[43] Wang JY, Yang SY, Huang YL, Tien HW, Chin WK, Ma CCM. Preparation and properties of graphene oxide/polyimide composite films with low dielectric constant and ultrahigh strength *via* in situ polymerization. J Mater Chem 2011;21(35):13569–75.
[44] Lei X, Chen Y, Qiao M, Tian L, Zhang Q. Hyperbranched polysiloxane (HBPSi)-based polyimide films with ultralow dielectric permittivity, desirable mechanical and thermal properties. J Mater Chem C 2016;4(11):2134–46.
[45] Li Q, Chen L, Gadinski MR, Zhang S, Zhang G, Li HU, et al. Flexible high-temperature dielectric materials from polymer nanocomposites. Nature 2015;523(7562):576.